Environ. Sci. Technol. **2005**, *39,* 7077−7083

Uranium Reduction in Sediments under Diffusion-Limited Transport of Organic Carbon

TETSU K. TOKUNAGA,*,† JIAMIN WAN,† JASQUELIN PENA,‡ EOIN L. BRODIE,† MARY K. FIRESTONE,‡ TERRY C. HAZEN,† STEVE R. SUTTON,§ ANTONIO LANZIROTTI,§ AND MATTHEW NEWVILLE§

Lawrence Berkeley National Laboratory, Berkeley, California 94720, University of California, Berkeley, California 94720, and University of Chicago, Chicago, Illinois 60637

Costly disposal of uranium (U) contaminated sediments is motivating research on in situ U(VI) reduction to insoluble U(IV) via directly or indirectly microbially mediated pathways. Delivery of organic carbon (OC) into sediments for stimulating U bioreduction is diffusion-limited in less permeable regions of the subsurface. To study OC-based U reduction in diffusion-limited regions, one slightly acidic and another calcareous sediment were treated with uranyl nitrate, packed into columns, then hydrostatically contacted with tryptic soy broth solutions. Redox potentials, U oxidation state, and microbial communities were well correlated. At average supply rates of 0.9 μmol OC (g sediment)$^{-1}$ day^{-1}, the U reduction zone extended to only about 35−45 mm into sediments. The underlying unreduced U(VI) zone persisted over 600 days because the supply of OC was diffusion-limited and metabolized within a short distance. These results also suggest that low U concentrations in groundwater samples from OC-treated sediments are not necessarily indicative of pervasive U reduction because interior and exterior regions of such sediment blocks can contain primarily U(VI) and U(IV), respectively.

Introduction

Uranium (U) is an important subsurface contaminant at sites associated with its mining and processing for energy and weapons production (*1*, *2*). Because of its high solubility under acidic and alkaline conditions, leakage of such extreme pH U solutions can lead to extensive contamination of soils and sediments. The high costs of excavating and disposing soils and sediments contaminated with U, as well as other actinides and metals, have motivated consideration of less expensive in-place treatment strategies that transform contaminants into insoluble forms.

A general approach under development for in-situ remediation of U-contaminated sediments involves stimulation of indigenous microorganisms to bioreduce mobile U(VI) to insoluble U(IV) by injection of easily metabolized forms of organic carbon (OC) (*3*, *4*). The common presence of high concentrations of nitrate as a co-contaminant with U complicates this strategy because denitrification and depletion of denitrification intermediates such as NO, NO_2^-, and N_2O reduction need to occur before significant U reduction is effective (*5*−*7*). Nitrate not only inhibits U(VI) reduction, but also serves as an electron acceptor for U(IV) oxidation (*6*, *7*). Addition of OC in high nitrate sediments has been reported to decrease U(VI) concentrations in solution, presumably through precipitation of U(VI) rather than U(IV) solid phases (*8*).

Effective distribution of OC in the subsurface remains a challenging technical problem. In bioremediation of subsurface contaminants, injection of OC solutions can result in permeability reduction within the delivery zone because of biofilm buildup (*9*). Periodic OC injection is one strategy that may minimize such fouling from biofilm growth (*10*). In addition, modeling studies indicate that pulsed nutrient injection can result in more effective remediation (*11*). An alternative strategy now being applied involves injection of a concentrated source of polymeric OC that slowly releases monomeric OC (*12*).

Regardless of the method of introduction into contaminated groundwater, OC will preferentially move through sparse networks of interconnected higher permeability flow paths, thereby largely bypassing most of the contaminated fractured sediment (Figure 1). While decades of time since contamination events allow U and other contaminants to become more uniformly distributed throughout sediments, short-term infusion of OC into the subsurface can be inefficient because of the combination of small regions associated with high flow networks and much larger volumes in which transport is diffusion-limited (*13*, *14*). Whether transport is advective or diffusive, the delivery of OC can be delayed further by sorption (*15*−*17*). Because groundwater monitoring employed during remediation relies on advection, it also preferentially samples regions along higher permeability networks. Unreduced U(VI) residing in lower permeability regions remains diffusively mobile and therefore available to migrate back into preferential flow paths when OC delivery is no longer maintained.

This laboratory study was designed to determine where U reduction occurs within diffusion-limited domains, whether high concentrations of unreduced U(VI) can coexist in diffusion-limited regions with U(IV)-dominated zones, and whether microbial communities are spatially correlated with U redox status within diffusion-limited systems.

Methods

The field-scale context of this laboratory experiment is that of periodic OC solution injection into U(VI)-contaminated sediments, with our focus on U redox transformations within lower permeability matrix blocks where OC is decomposed while it diffuses in from higher permeability channels (Figure 1b). Thus, we are concerned with local OC transport and subsequent redox reactions along transects starting at fracture−matrix boundaries, and moving into interior regions of sediment blocks.

Sediment Columns. The interaction between advectively accessible preferential transport paths and low permeability sediment regions is represented in the laboratory model by placement of an OC solution reservoir in hydrostatic contact (ponded at atmospheric pressure) over one end of a small sediment column (12.7 mm diameter, approximately 55 mm length, Figure 1c). The column design and sediments used were described in companion studies on U(VI) diffusion (*18*) and sorption (*19*). Solutions containing 3 mM $UO_2(NO_3)_2$

* Corresponding author phone: (510)486-7176; fax: (510)486-7797; e-mail: tktokunaga@lbl.gov.
† Lawrence Berkeley National Laboratory.
‡ University of California.
§ University of Chicago.

10.1021/es050221a CCC: $30.25
Published on Web 08/13/2005

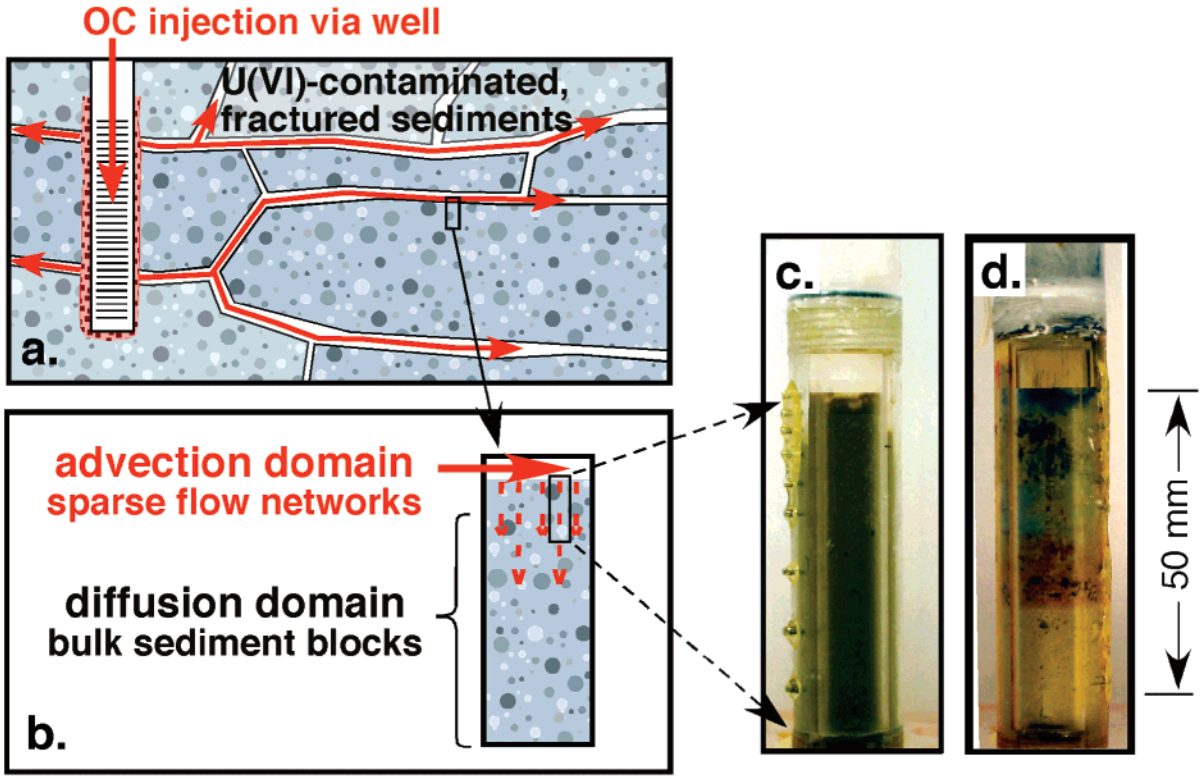

FIGURE 1. Conceptual models of (a) preferential flow and OC transport along interconnected fracture paths after injection through a well (not to scale), and (b) diffusion-limited transport of OC into sediment blocks. (c,d) Photographs of laboratory U-contaminated sediment columns, without and with 67 mM OC solutions, respectively.

TABLE 1. Properties of the Oak Ridge and Altamont Sediments Used in the Experiments[a]

	units	Altamont	Oak Ridge
sand	mass %	10	45
silt	mass %	62	43
clay	mass %	28	12
calcium carbonate equivalent	mass %	10	0.1
total Fe (XRF)	mass %	4.5	4.6
0.5 M HCl extractable Fe	mass %	0.24	0.37
pH (pore water prior to U exposure)		8.0 ± 0.2	6.2 ± 0.5
electrical conductivity	μS cm^{-1}	300	30
Ca^{2+}	mM$_c$	1.65	0.19
Mg^{2+}	mM$_c$	1.13	0.04
Na^{+}	mM$_c$	0.33	0.11
K^{+}	mM$_c$	0.04	0.01
SO_4^{2-}	mM$_c$	0.11	0.06
HCO_3^{-}	mM$_c$	1.68	0.15
Cl^{-}	mM$_c$	0.24	0.08
NO_3^{-}	mM$_c$	1.29	0.08

[a] Solution chemistry data are from 1:1 water:sediment extracts. Additional details are available in Zheng et al. (*19*).

were adjusted to either pH 2 or pH 12, with HCl or NaOH. Each solution was then mixed into two different initially air-dry sediments, one from Oak Ridge National Laboratory, TN (denoted OR2 and OR12 for pH 2 and pH 12 uranyl solutions, respectively), and the other from Altamont Pass, CA (denoted AL2 and AL12). Some basic properties of the sediments are summarized in Table 1. A solution:sediment mass ratio of 0.45 ± 0.05 was prepared for each sediment, and wet-packed into columns. This gave a bulk density of 1.21 ± 0.07 Mg m^{-3}, porosity of 0.55 ± 0.02, and an initial U(VI) concentration of 323 ± 36 μg (g sediment)$^{-1}$ (1.36 ± 0.15 μmol (g sediment)$^{-1}$). Initial sediment pore water NO_3^- concentrations were 6.2 and 9.0 mM for the OR and AL sediments, respectively (AL having a high native NO_3^- concentration).

The sediment columns were maintained under hydrostatic conditions (sealed at the bottom to prevent outflow), with OC solutions of tryptic soy broth (TSB) periodically applied by pooling at the top surface of the sediments. The OC reservoir consisted of a 9.0 mL capacity, 71 mm tall cylindrical extension above the main sediment column (*18*). These solutions had OC concentrations of 0, 6.7, and 67 mM when initially dispensed onto the upper surface of sediments. Each application involved first withdrawing the previously pooled solution with a syringe, and then replacing it with 9.0 mL of one of the OC solutions. These applications amounted to adding 0, 6.3, or 63 μmol OC per g sediment, for the three different solutions. Individual columns received the same type of solution each time, for a total of eight recharge times over the 20-month experiment (2−4 month intervals). Variation in recharge intervals allowed for observation of redox electrode responses. This rate of solution replacement was equivalent to average supply rates of 0, 0.09, and 0.9 μmol OC (g sediment)$^{-1}$ day^{-1}.

Upon placement at the upper boundary of a sediment column, OC transport into the sediment is controlled by diffusion, sorption, and degradation. Because the OC of TSB is initially in the form of partially hydrolyzed proteins, and because it is oxidized while diffusing, it does not have a unique diffusivity in sediments. For later comparisons, a range of effective diffusivities of OC in our sediment was estimated by applying the Scheibel correlation (*20*) to molecules ranging in size from 600 Da (~5 peptide chain) to 60 Da (acetate). Using a diffusibility of 0.68 (*18*), calculated effective diffusivities, D_e, are in the range of 1.3×10^{-10} to 4.5×10^{-10} m^2 s^{-1}.

Each column was monitored through measurements in its reservoir (pH, U, and OC concentrations) and sediment (redox potential, U(VI) and U(IV) concentrations). pH

measurements were obtained by inserting a combination electrode into the reservoir. Uranium and OC concentrations within reservoirs were measured by kinetic phosphorimetry (KPA, Chemchek) and by persulfate oxidation (model 1010 TIC-TOC Analyzer, O.I. Analytical), respectively. Redox potentials within each sediment column were obtained with sets of nine embedded 0.8 mm diameter Pt electrodes (*18*).

X-ray Absorption Spectroscopy. Concentration profiles for U(VI) and U(IV) were obtained by micro-X-ray absorption near edge structure (μ-XANES) spectroscopy (*21*). One side of each column wall was milled to a thickness of 1.0 mm to minimize absorption of incident and fluorescent X-rays. A wide incident beam size (about 0.2 mm vertical $\times$ 1.0 mm horizontal) was used to obtain oxidation states averaged over many grains, surfaces, and pores at each measurement location. These measurements were obtained on day 257 at beamline X26A of the National Synchrotron Light Source, and on days 150, 361, and 600 at the GSECARS microprobe beamline 13-ID, Advanced Photon Source. The U(VI) fractions in sediments were determined by comparing their U L_{III} absorption edge energies at half step height to those of reference compounds (*22*). Our reference compounds were UO_2 powder diluted to 1% in silica powder, and a 4 mM $UO_2(NO_3)_2$ aqueous solution. Concentrations of total U were determined from magnitudes of the U L_{III} absorption edge step (before normalization to unit magnitude).

Microbiology. Columns were sampled aseptically in an anaerobic glovebox after day 638, by cutting open lengthways using a sterilized blade and sectioning sediments (5 mm intervals) aseptically using a sterilized scalpel. DNA was extracted from 0.5 g of sediment using the FastDNA Spin Kit (QBiogene, CA), and bacterial community structure was assessed using terminal restriction fragment length polymorphism (T-RFLP) analysis of bacterial 16S rRNA genes (*23*). Microbial activity (dehydrogenase) was measured anaerobically using an INT reduction assay (*24*) with 0.1 g of sediment. For T-RFLP analysis, DNA was quantified using PicoGreen (Molecular Probes, OR), and 16S rRNA gene amplification was performed using bacterial primers 27F and 1492R (*25*). PCR was performed in triplicate for each section with amplicons pooled for each extract. Approximately 400 ng of amplicon was digested overnight at 37 °C with endonuclease *Alu*I (NEB, MA). Digested amplicons were resuspended in formamide, and aliquots were mixed with GeneScan 500-Rox size standard. Electrophoresis was carried out using an ABI 3100 automated capillary sequencer (Applied Biosystems, CA) run in GeneScan mode. Terminal restriction fragments (TRFs) were sized using GeneScan v3.7 software. TRFs were considered identical if they differed by <0.5 bp. Individual TRF heights were normalized as a percent of total peak height.

To visualize patterns in bacterial community structure, T-RFLP data were subjected to principal component analysis, and the first two components were plotted (PC1 and PC2). To determine if microbial activity and community structure (PC1 and PC2) along the column profile were associated with redox potential or U oxidation state, Pearson correlation coefficients were calculated for these parameters. Only data for Altamont sediments receiving high concentrations of OC (67 mM) are presented here.

Results and Discussion

All columns treated with 6.7 mM OC showed no significant differences in redox potentials and U oxidation state relative to the +0 OC treatments, indicating that nitrate concentrations in the sediments and rates of dissolved oxygen diffusion were high enough to react with this lower level of OC. Therefore, only comparisons between +0 and +67 mM OC will be presented here.

pH. Reservoir solutions stabilized to pH values (Figure S1, Supporting Information) that reflected influences of the initial U(VI) solution pH, sediment properties (Table 1), and redox reactions. The pH 2 solution initially equilibrated to the slightly acidic range (pH 6.0 $\pm$ 1.0) in the weakly buffered (low $CaCO_3$) OR sediments. The most influential sediment property was the calcium carbonate concentration, especially in the AL sediments. Buffering by $CaCO_3$ brought all AL and the initially pH 12 OR reservoir solution pH values to 8.0 $\pm$ 0.5 within the first 40 days. The initially pH 2 OR sediment remained slightly acidic (pH 6.0 $\pm$ 1.0) without addition of OC (as well as with 6.7 mM OC), but the corresponding system treated with 67 mM OC had its pH increase over the first 40 days to a final level of 7.6 $\pm$ 0.8. The OC-dependent pH increase in the pH 2 OR sediment treated with the highest OC solution probably resulted from Fe(III) and Mn(IV) reduction. Both of these reduction reactions consume protons and efficiently raise pH during OC oxidation (*26*). In all of these sediments, rapid neutralization of the extreme initial pH values (2 and 12) of the original U solutions resulted in rapid loss of U(VI) from solution. Because U(VI) solubilities at circum-neutral pH are in the micromolar range, most of the U was sorbed or precipitated in U(VI) forms upon initial mixing into sediments.

Sorption of Organic Carbon. The sorption partitioning coefficient, K_d, in the AL sediment was nearly constant at 6.8 mL g^{-1} for TSB and 5.2 mL g^{-1} for lactate, up to OC concentrations of 100 mM (Figure S2, Supporting Information). In the OR sediment, OC sorption was weakly nonlinear, ranging from 10 to 7 mL g^{-1} for TSB, and from 8 to 5.5 mL g^{-1} for lactate as the OC concentration was increased (Figure S2, Supporting Information). The magnitude of TSB sorption was similar to that of many individual amino acids on smectite (*15*), and much lower than that reported for proteins on smectite (*16*), which can have effective K_d values of $\sim 10^2$ mL g^{-1}. Lactate sorption on these two sediments was slightly weaker than TSB sorption, with differences becoming insignificant at higher concentrations. Because of pH-dependence of sorption, these measurements are more directly applicable to the AL sediment columns (pH 8.0 $\pm$ 0.5) and the acidic OR columns (pH 6.0 $\pm$ 1.0). For the more alkaline OR sediments, OC sorption is expected to be weaker than the measured values obtained at pH 4.9 $\pm$ 0.5 because of increased electrostatic repulsion (*17*).

Redox Potentials. Redox potential measurements showed continuously oxidizing conditions in sediments lacking OC addition. Decreases in redox potentials were observed in shallow sediments directly adjacent to the reservoirs shortly after all OC additions, while deeper regions of these OC-treated systems remained oxidizing (Figure S3, Supporting Information). It should be kept in mind that Pt electrode sensitivity to the different redox couples is quite varied and that the various redox couples are in disequilibrium (*1*). Analyses of OC in reservoirs indicated about 95 $\pm$ 2% depletion within 75 days, and 98 $\pm$ 1% depletion by 100 days following recharge times. Redox profile responses to three of the OC application events (days 243, 320, and 579) are shown in Figure 2. All but three electrodes (data circled in Figure 2c and 2l) appeared responsive throughout the experiment. The need to periodically replenish OC to sustain reducing conditions is reflected in the tendency of redox potentials to return to otherwise high levels. Depth profiles of redox potentials reflected diffusion-limited OC transport and degradation. The reduction front reached depths of about 35−45 mm with the periodic OC applications. The deepest regions of these columns remained continuously oxidizing throughout the experiment. The presence of high concentrations of NO_3^- was important in sustaining oxidizing conditions, as it is in field sediments where it is often a co-contaminant with U. These redox data show that when characteristic sediment block sizes are large, substantial

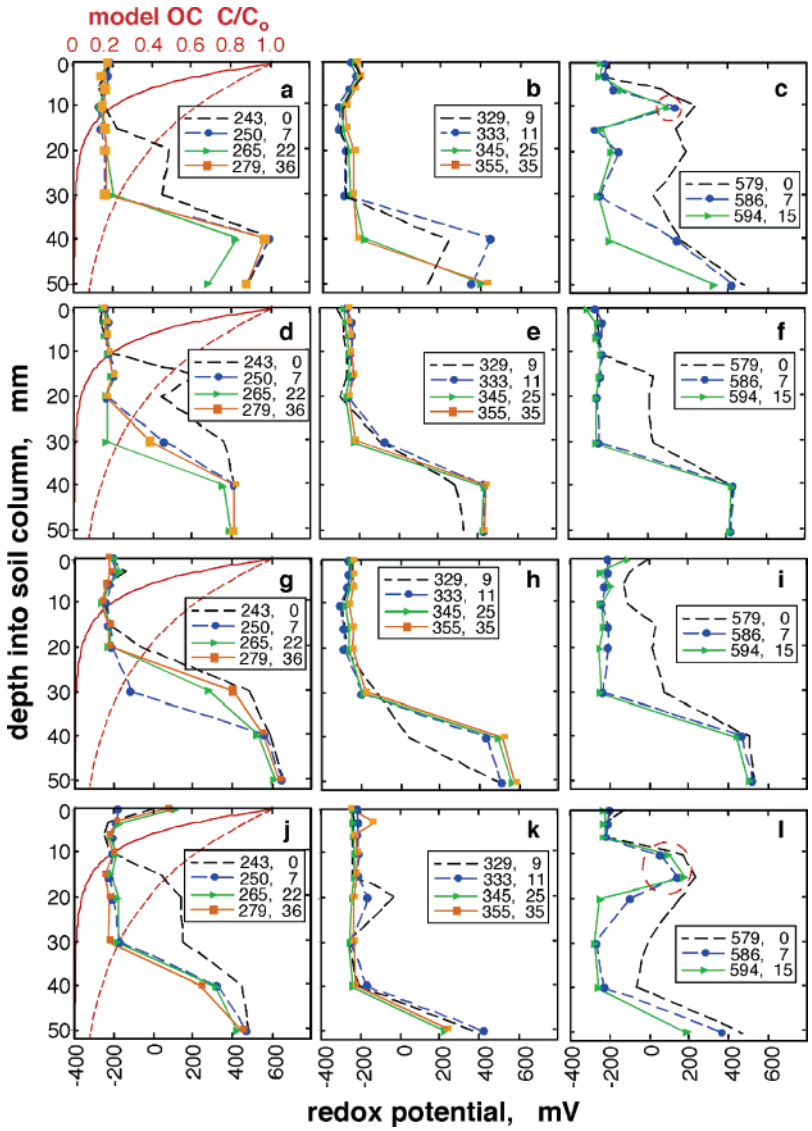

FIGURE 2. Depth profiles of redox potentials in columns periodically exposed to 67 mM OC. Sediments are AL2 (a,b,c), AL12 (d,e,f), OR2 (g,h,i), and OR12 (j,k,l). Total elapsed time (days) and days since latest OC addition are indicated in legends. Redox potentials are referenced to the standard H electrode (uncertainties ≈ ±60 mV). Anomalous redox values at later times are encircled in frames c and l. The red curves in panels a, d, g, and j show calculated steady-state OC profiles for first-order OC oxidation with constant boundary OC concentration of 33.5 mM (eq 1), for $D_e = 1.3 \times 10^{-10}$ (solid) and 4.5×10^{-10} m^2 s^{-1} (dashed).

volumes of oxidizing sediments can persist in field sites injected with OC, coexisting with reducing sediments and waters.

Estimated OC Diffusion Profiles. The measured redox potential profiles in the OC-treated sediments were relatively stable despite the periodic variation of OC at the upper boundary. This motivated a comparison between these redox profiles and a calculated steady-state profile for OC diffusion and oxidation. Because the reservoir OC concentration varied periodically between 67 mM at times of reservoir replenishment and 2 ± 2 mM at the end of each OC depletion cycle, the equivalent constant boundary OC concentration, C_o, was taken as 33.5 mM, half the periodically applied concentration. The steady-state OC concentration profile under these ideal conditions, and with the simplification of first-order OC oxidation kinetics, is given by (*27*):

$$\frac{C(x)}{C_o} = \exp[x\sqrt{k/D_e}] \qquad (1)$$

where x is the depth, D_e is set equal to 1.3×10^{-10} to 4.5×10^{-10} m^2 s^{-1}, as described earlier, and k is the effective first-order OC oxidation rate. The column-averaged OC supply rate of 0.9 μmol (g sediment)$^{-1}$ day^{-1} was scaled with D_e (*27*) to obtain k, ranging from 0.32 to 0.093 day^{-1}, for the lower and higher values of D_e, respectively. The calculated steady-state OC profiles are superimposed on the 243−279 day data in Figure 2 for comparisons with the redox potential profiles. Note that, although OC sorption is significant in our sediments, neither sorption (K_d) nor porosity appears in eq 1 because storage (capacity) terms influence transient but not steady-state diffusion. Although the steady state and first-order model is a simplification of our experiment, the locations of the measured redox boundaries are fairly well constrained by these calculations.

U Oxidation States. Profiles of U oxidation states in the sediment columns obtained by μ-XANES spectroscopy were usually consistent with the Pt electrode measurements, with U reduction largely occurring within the redox potential range of −0.20 ± 0.05 V (Figure S4, Supporting Information). Sediments that were not treated with high OC solutions exhibited insignificant reduction; that is, U(VI) accounted for at least 93% of the total U (data not shown). In contrast, sediment columns that were periodically exposed to high

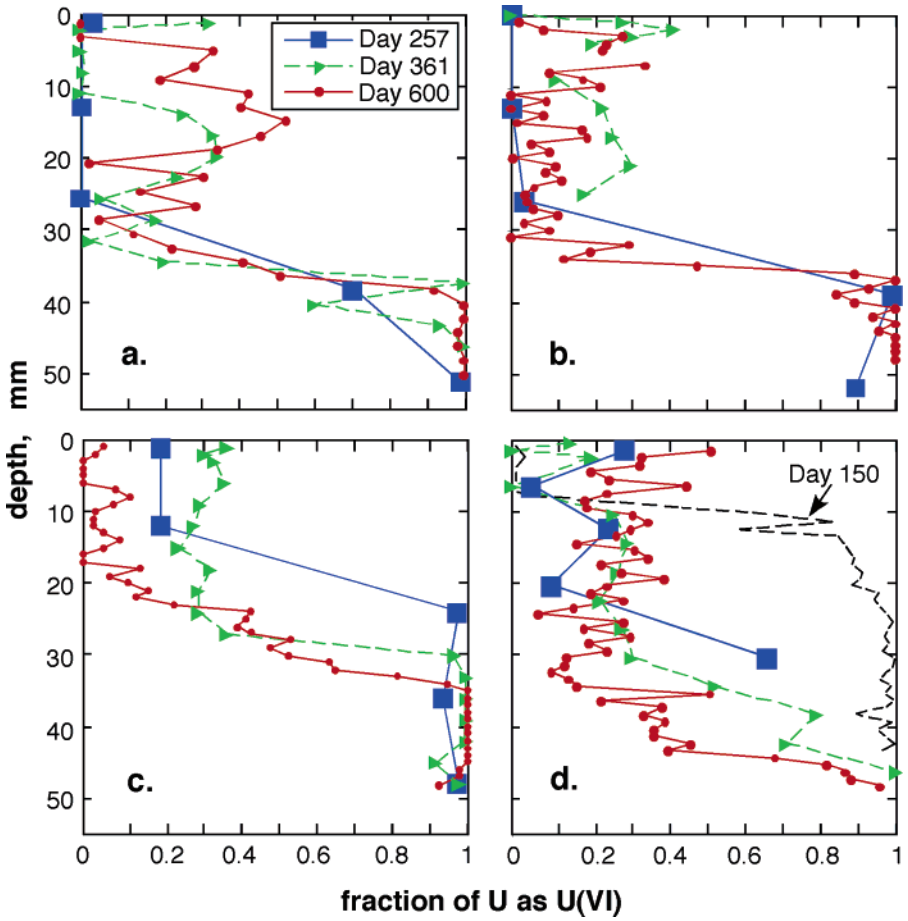

FIGURE 3. U oxidation state profiles, determined by micro-X-ray absorption spectroscopy, for (a) AL2, (b) AL12, (c) OR2, and (d) OR12 sediments exposed to 67 mM OC solutions. Absolute uncertainties in U(VI) fractions ≈ 0.12.

(67 mM) concentrations of OC experienced U reduction in regions closest to the OC source. Oxidation state profiles, showing the fraction of total U occurring as U(VI) at various depths in sediment columns, U(VI)/∑U, are presented in Figure 3 (absolute uncertainties in U(VI) fractions ≈ ±0.12). Micro-XANES spectra were obtained on all sediments on days 257, 361, and 600, but only the OR12 sediment on day 150. Comparisons of that U oxidation state profile with profiles obtained at later times (Figure 3d) indicate that the U reduction front was advancing relatively rapidly up to some time between days 150 and 257, and thereafter remained within depths of 35−45 mm. Thus, the periodic OC treatments established stable U redox stratification with reduced U(IV)-dominated sediments closest to the OC source, overlying the deeper region containing unreduced U(VI). Note that information on U redox stratification would be unavailable from any bulk sediment analyses that average over several centimeter distances.

Although U was predominantly maintained as U(IV) in near-surface sediments exposed to 67 mM OC solutions, reduction to U(IV) was not complete in these reduced zones (Figure 3). Recalcitrant fractions of U that persist as U(VI) in reducing sediments have been reported recently (*28*−*30*). In addition, U(IV) reoxidation can be promoted under some OC-stimulated reducing conditions because elevated P_{CO_2} from microbial respiration enhances solubilization of U(VI) by carbonate complex formation (*31*).

Redox-Driven U Transport. Total U profiles in sediment columns at the end of the experiment are shown in Figure 4. Without OC, total U profiles remained fairly uniform. In contrast, redistribution of U was observed in the Altamont sediments supplied with 67 mM OC, and to a lesser extent

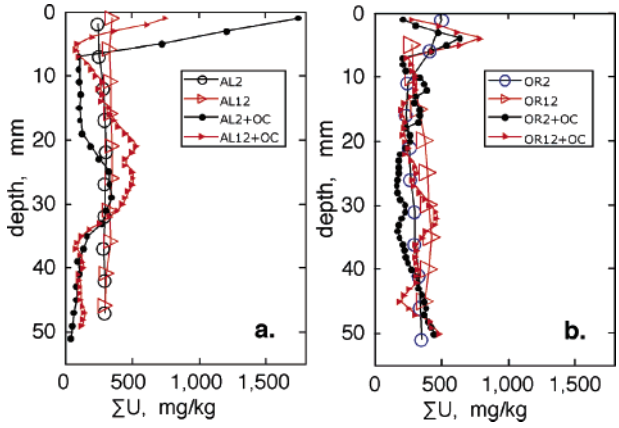

FIGURE 4. Profiles of total U concentrations in (a) Altamont and (b) Oak Ridge sediments at day 600. Sediments exposed to 67 mM OC solutions are indicated by "+OC".

in the similarly treated Oak Ridge sediment. Because of the complex biogeochemistry of U, including unknown rate laws and their constants, and variable boundary conditions, reactive transport modeling is beyond the scope of this study. Nevertheless, basic aspects of the measured U redistribution can be addressed. Uranium concentration maxima developed at or near the OC-treated surfaces, indicative of U(VI) diffusion toward the surface region where rates of OC oxidation and U(VI) reduction were probably highest. The sustained steep gradients in redox potential and U(VI)/∑U at about the 40 mm depth in the sediments treated with high concentrations of OC indicate that diffusion of redox-sensitive species continued to occur across this zone up to 600 days.

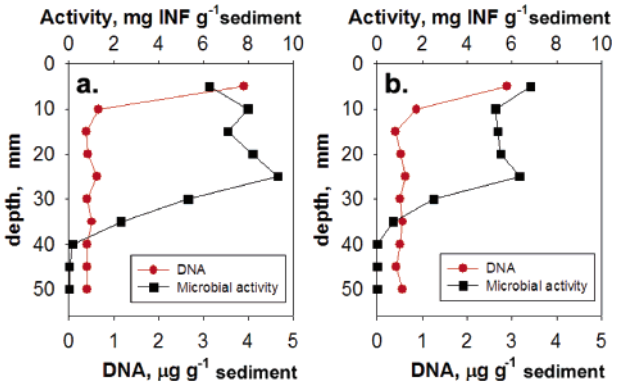

FIGURE 5. Microbial biomass and activity along Altamont column profiles from sediments previously contaminated with (a) pH 2 and (b) pH 12 uranyl nitrate solutions.

Thus, transport of NO_3^-, Fe^{2+}, and aqueous U(VI) carbonate species is inferred. We could not measure NO_3^- in these small sediment columns, but the redox electrodes indicate that Fe(III) reduction did not occur beyond ~40 mm depth. Diffusive/reductive loss of NO_3^- (initially 6−9 mM) may have been too slow to allow Fe(III) reduction to occur below this depth. Diffusion of Fe(II) from the shallower reducing sediment to the oxidizing deeper region was qualitatively evident from formation of red-orange Fe(III) precipitates in the 35−45 mm depths (e.g., Figure 1d). Diffusion of U(VI) from the deeper region into the overlying reducing zone was clearly observed in the AL sediments supplied with 67 mM OC (Figure 4a), but not in the OR sediments (Figure 4b).

Higher mobility of U(VI) in the AL sediments (Figure 4a) than in the OR sediments (Figure 4b) was evident from magnitudes of their concentration maxima in the surface region and from differences in their concentration profiles at greater depths. This is consistent with much weaker U(VI) sorption measured on the AL sediments relative to the OR sediments in the range of pH 7−8 (*19*), resulting in higher apparent U(VI) diffusivities in the AL sediments (*18*). Because the AL sediment contains a large fraction of $CaCO_3$ (10%) and the OR has very little $CaCO_3$ (~0.1%), and because the very stable aqueous $Ca_2UO_2(CO_3)_3$ species (*32*) appears to be responsible for minimizing U(VI) sorption (*19*), we believe that $Ca_2UO_2(CO_3)_3$(aq) is responsible for the greater U(VI) mobility observed in the AL sediments. Although the value of the $Ca_2UO_2(CO_3)_3$(aq) formation constant is provisional (*33*), the present results indicate that higher U(VI) mobility in $CaCO_3$ rich environments may be attributed to the strength of this complex. Other recent studies have indicated that the stability of $Ca_2UO_2(CO_3)_3$(aq) is important in slowing rates of U bioreduction (*34*) and that this species also occurs in U(VI)-contaminated sediments at the Hanford Site (*35*).

Bacterial Community Analyses. Analyses from the Altamont sediments are presented here. More detailed analyses of the effects of contaminant solution pH and organic carbon diffusion in Oak Ridge sediment microbial communities are to be provided in an upcoming manuscript. Using DNA as a proxy for biomass, it was clear that microbial biomass accumulated near the sediment surface (Figure 5a,b). Concentration of biomass at the point of carbon addition is expected and is a significant concern in subsurface remediation strategies as it may lead to permeability reduction and also alter diffusion/consumption dynamics. However, despite the sharp decline in biomass within 5 mm of the surface, microbial activity remained at high levels for up to 30 mm from the point of carbon addition (Figure 5a,b), confirming the diffusion of OC to this depth. Activity was well correlated with redox potential only in the sediment contaminated initially with pH 12 uranyl nitrate, but in both treatments the proportion of U as U(VI) was significantly correlated with microbial activity (Table S1, Supporting Information).

16S T-RFLP analysis indicated a distinct divergence in bacterial communities throughout the length of the columns (Figure S5a,b, Supporting Information). Bacterial communities near the sediment surface clustered separately from communities elsewhere along the column, while those in deeper regions (>35 mm) also clustered separately. To further investigate the parameters associated with microbial stratification, we tested for correlations between two significant geochemical parameters, redox potential and U speciation (oxidation state), and ordination values reflecting bacterial community structure, principal components 1 and 2 (Table S1, Supporting Information). This approach has been used previously to associate patterns in microbial structure with concentrations of hydrocarbons, lead, and chromate (*36*).

While redox potential was only correlated with bacterial community structure in the pH 12 treatment, U speciation was highly correlated with bacterial community structure in sediments irrespective of starting contaminant solution pH. The presence of distinct communities in the surface sections was expected given that these regions experienced the highest OC, had greater biomass, and had higher U concentrations. Conversely, from redox data it appears that communities present in deeper oxidizing regions (40−50 mm) did not receive significant OC, probably as a result of diffusion/consumption-limited transport. These two factors (OC and U concentration) would impose a significant selective pressure on bacterial communities. Because the sediments were co-contaminated with nitrate, small quantities of OC diffusing into the interface of the reducing and oxidizing regions would likely be oxidized with nitrate as the terminal electron acceptor. Denitrification intermediates such as NO, NO_2^-, and N_2O are known to reoxidize U(IV) (*5*), and this may be an additional factor in retarding the U reduction front in the lower column regions. These data suggest that distinct bacterial communities are associated with the regions of reduced and oxidized U, and the composition of these communities may functionally impact the solubility of U and its flux between reducing and oxidizing regions.

Implications for OC-Based in Situ U Reduction. This study shows that, in diffusion-limited regions of the subsurface, reductive U precipitation zones can remain restricted within a few centimeters of OC delivery flow paths. Stratification of redox potentials, microbial communities, and U oxidation state can be very distinct and well correlated. Regions within structurally heterogeneous sediments can retain unreduced U(VI) after more advectively accessible regions along flow paths have undergone U bioreduction. This is especially true when NO_3^- or other oxidants are present as a co-contaminant with U. Where monitoring of remediation involves preferentially sampling from more permeable and treatable regions of the subsurface, inventories of unreduced U in less conductive regions may be underestimated. Finally, even when thorough U reduction is achievable, its sustainability in regionally oxidizing environments needs to be examined given the long half-life of ^{238}U (4.5×10^9 years).

Acknowledgments

We thank Keith Olson, Don Herman, Yongtian Tom He, Andrew Mei, Bill Rao, Geoff McCool, and the GSECARS staff for technical assistance, and David Watson and the Natural and Accelerated Bioremediation Research (NABIR) Program, Field Research Center staff, for samples of Oak Ridge sediments. Internal review comments by Zuoping Zheng and helpful comments by Associate Editor Janet Hering and reviewers are gratefully acknowledged. Funding was provided by the U.S. Department of Energy, Basic Energy Sciences,

Geosciences Program, and the NABIR Program, under contract No. DE-AC03-76SF00098. Portions of this work were performed at GeoSoilEnviroCARS (Sector 13), Advanced Photon Source (APS), Argonne National Laboratory. GeoSoilEnviroCARS is supported by the National Science Foundation − Earth Sciences (EAR-0217473), Department of Energy − Geosciences (DE-FG02-94ER14466), and the State of Illinois. Use of the APS was supported by the U.S. Department of Energy, Basic Energy Sciences, Office of Energy Research, under Contract No. W-31-109-Eng-38.

Supporting Information Available

Additional material on organic carbon sorption measurements, correlations of bacterial structure and activity with environmental parameters (Table S1), pH trends (Figure S1), OC sorption partition coefficients (Figure S2), redox potential time series (Figure S3), U oxidation state correlation with redox potential (Figure S4), and bacterial community structure profiles (Figure S5). This material is available free of charge via the Internet at http://pubs.acs.org.

Literature Cited

(1) Langmuir, D. *Aqueous Environmental Geochemistry*; Prentice Hall: Upper Saddle River, 1997.

(2) Riley, R. G.; Zachara, J. M.; Wobber, F. J. *Chemical Contaminants on DOE Lands and Selection of Contaminant Mixtures for Subsurface Science Research*; U.S. Department of Energy: Washington, DC, 1992.

(3) Finneran, K. T.; Anderson, R. T.; Nevin, K. P.; Lovley, D. R. Potential for bioremediation of uranium-contaminated aquifers with microbial U(VI) reduction. *Soil Sediment Contam.* **2002**, *11*, 339−357.

(4) Anderson, R. T.; Vrionis, H. A.; Ortiz-Bernad, I.; Resch, C. T.; Long, P. E.; Dayvault, R.; Karp, K.; Marutzky, S.; Metzler, D. R.; Peacock, A.; White, D. C.; Lowe, M.; Lovley, D. R. Stimulating the in situ activity of Geobacter species to remove uranium from the groundwater of a uranium-contaminated aquifer. *Appl. Environ. Microbiol.* **2003**, *69*, 5884−5891.

(5) Senko, J. M.; Istok, J. D.; Suflita, J. M.; Krumholz, L. R. In-situ evidence for uranium immobilization and remobilization. *Environ. Sci. Technol.* **2002**, *36*, 1491−1496.

(6) Finneran, K. T.; Housewright, M. E.; Lovley, D. R. Multiple influences of nitrate on uranium solubility during bioremediation of uranium-contaminated subsurface sediments. *Environ. Microbiol.* **2002**, *4*, 510−516.

(7) Istok, J. D.; Senko, J. M.; Krumholz, L. R.; Watson, D.; Bogle, M. A.; Peacock, A.; Chang, Y.-J. White, D. C. In situ bioreduction of technetium and uranium in a nitrate-contaminated aquifer. *Environ. Sci. Technol.* **2004**, *38*, 468−475.

(8) Shelobolina, E. S.; O'Neill, K.; Finneran, K. T.; Hayes, L. A.; Lovley, D. R. Potential for in situ bioremediation of a low-pH, high nitrate uranium-contaminated groundwater. *Soil Sediment Contam.* **2003**, *12*, 865−884.

(9) Baveye, P.; Vandevivere, P.; Hoyle, B. L.; Deleo, P. C.; Delozada, D. S. Environmental impact and mechanisms of the biological clogging of saturated soils and aquifer materials. *Crit. Rev. Environ. Sci. Technol.* **1998**, *28*, 123−191.

(10) Peyton, B. M. Improved biomass distribution using pulsed injections of electron donor and acceptor. *Water Res.* **1996**, *30*, 756−758.

(11) Phanikumar, M. S.; Hyndman, D. W. Interactions between sorption and biodegradation: Exploring bioavailability and pulsed nutrient injection efficiency. *Water Resour. Res.* **2003**, *39*, 1122.

(12) Haas, J. E.; Trego, D. A. A field application of hydrogen-releasing compound for the enhanced bioremediation of methyl tertiary butyl ether. *Soil Sediment Contam.* **2001**, *10*, 555−575.

(13) Gerke, H. H.; van Genuchten, M. T. Macroscopic representation of structural geometry for simulating water and solute movement in dual porosity media. *Adv. Water Resour.* **1996**, *19*, 343−357.

(14) Jorgensen, P. R.; Helstrup, T.; Urup, J.; Seifert, D. Modeling of nonreactive solute transport in fractured clayey till during variable flow rate and time. *J. Contam. Hydrol.* **2004**, *68*, 193−216.

(15) Hedges, J. I.; Hare, P. E. Amino acid adsorption by clay minerals in distilled water. *Geochim. Cosmochim. Acta* **1987**, *51*, 255−259.

(16) Harter, R. D.; Stotsky, G. Formation of clay-protein complexes. *Soil Sci. Soc. Am. Proc.* **1971**, *35*, 383−389.

(17) Filius, J. D.; Hiemstra, T.; Van Riemsdijk, W. H. Adsorption of small weak organic acids on goethite: Modeling of mechanisms. *J. Colloid Interface Sci.* **1997**, *195*, 368−380.

(18) Tokunaga, T. K.; Wan, J.; Pena, J.; Sutton, S. R.; Newville, M. Hexavalent uranium diffusion into soils from concentrated acidic and alkaline solutions. *Environ. Sci. Technol.* **2004**, *38*, 3056−3062.

(19) Zheng, Z.; Tokunaga, T. K.; Wan, J. Influence of calcium carbonate on U(VI) sorption to soils. *Environ. Sci. Technol.* **2003**, *37*, 5603−5608.

(20) Li, J.; Carr, P. W. Accuracy of empirical correlations for estimating diffusion coefficients in aqueous organic mixtures. *Anal. Chem.* **1997**, *69*, 2530−2536.

(21) Bertsch, P. M.; Hunter, D. B. Applications of synchrotron-based X-ray microprobes. *Chem. Rev.* **2001**, *101*, 1809−1842.

(22) Duff, M. C.; Morris, D. E.; Hunter, D. B.; Bertsch, P. M. Spectroscopic characterization of uranium in evaporation basin sediments. *Geochim. Cosmochim. Acta* **2000**, *64*, 1535−1550.

(23) Liu, W. T.; Marsh, T. L.; Cheng, H.; Forney, L. J. Characterization of microbial diversity by determining terminal restriction fragment length polymorphisms of genes encoding 16S rRNA. *Appl. Environ. Microbiol.* **1997**, *63*, 4516−4522.

(24) Von Mersi, W.; Schinner, F. An improved and accurate method for determining the dehydrogenase activity of soils with iodonitrotetrazolium chloride. *Biol. Fertil. Soils* **1991**, *11*, 216−220.

(25) Wilson, K. H.; Blitchington, R.; Greene, R. C. Amplification of bacterial 16S ribosomal DNA with polymerase chain reaction. *J. Clin. Microbiol.* **1990**, *29*, 1942−1946.

(26) Scott, M. J.; Morgan, J. J. Energetics and conservative properties of redox systems. In *Chemical Modeling of Aqueous Systems II*; Melchior, D. C., Bassett, R. L., Eds.; ACS Symp. Ser. 416; American Chemical Society: Washington, DC, 1990.

(27) Crank, J. *The Mathematics of Diffusion*, 2nd ed.; Oxford Press: Oxford, 1975.

(28) Jeon, B. H.; Kelly, S. D.; Kemner, K. M.; Barnett, M. O.; Burgos, W. D.; Dempsey, B. A.; Roden, E. E. Microbial reduction of U(VI) at the solid-water interface. *Environ. Sci. Technol.* **2004**, *38*, 5649−5655.

(29) Missana, T.; Garcia-Guitierrez, M.; Alonso, U. Kinetics and reversibility of cesium and uranium sorption onto bentonite colloids in a deep granitic environment. *Appl. Clay Sci.* **2004**, *26*, 137−150.

(30) Ortiz-Bernad, I.; Anderson, R. T.; Vrionis, H. A.; Lovley, D. R. Resistance of solid-phase U(VI) to microbial reduction during in situ bioremediation of uranium-contaminated groundwater. *Appl. Environ. Microbiol.* **2004**, *70*, 7558−7560.

(31) Wan, J.; Tokunaga, T. K.; Brodie, E.; Wang, Z.; Zheng, Z.; Herman, D.; Hazen, T. C.; Firestone, M. K.; Sutton, S. R. Reoxidation of bioreduced uranium under reducing conditions. *Environ. Sci. Technol.* **2005**, *39*, in press.

(32) Bernhard, G.; Geipel, G.; Reich, T.; Brendler, V.; Amayri, S.; Nitsche, H. Uranyl(VI) carbonate complex formation: Validation of the $Ca_2UO_2(CO_3)_3$(aq.) species. *Radiochim. Acta* **2001**, *89*, 511−518.

(33) Guillaumont, R.; Fanghanel, T.; Fuger, J.; Grenthe, I.; Neck, V.; Palmer, D. A.; Rand, M. H.; Mompean, F. J.; Illemassene, M.; Domenechi-Orti, C. *Update on the Chemical Thermodynamics of Uranium, Neptunium, Plutonium, Americium, and Technicium*; Elsevier: Amsterdam, 2003.

(34) Brooks, S. C.; Fredrickson, J. K.; Carroll, S. L.; Kennedy, D. W.; Zachara, J. M.; Plymale, A. E.; Kelly, S. D.; Kemner, K. M.; Fendorf, S. Inhibition of bacterial U(VI) reduction by calcium. *Environ. Sci. Technol.* **2003**, *37*, 1850−1858.

(35) Wang, Z.; Zachara, J. M.; Yantasee, W.; Gassman, P. L.; Liu, C.; Joly, A. G. Cryogenic laser induced fluorescence characterization of U(VI) in Hanford vadose zone pore waters. *Environ. Sci. Technol.* **2004**, *38*, 5591−5597.

(36) Shi, W.; Becker, J.; Bischoff, M.; Turco, R. F.; Konopka, A. E. Association of microbial community composition and activity with lead, chromate, and hydrocarbon contamination. *Appl. Environ. Microbiol.* **2002**, *68*, 3859−3866.

Received for review February 2, 2005. Revised manuscript received July 15, 2005. Accepted July 18, 2005.

ES050221A